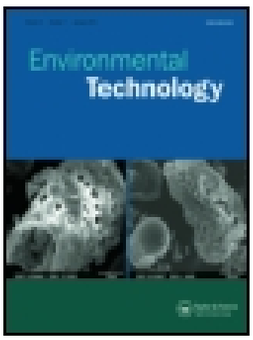

Environmental Technology

ISSN: 0959-3330 (Print) 1479-487X (Online) Journal homepage: http://www.tandfonline.com/loi/tent20

Synthesis, characterization, and photocatalytic activity of sonochemical/hydration–dehydration prepared ZnO rod-like architecture nano/microstructures assisted by a biotemplate

Ayad F. Alkaim, Enas M. Alrobayi, Abrar M. Algubili & Aseel M. Aljeboree

To cite this article: Ayad F. Alkaim, Enas M. Alrobayi, Abrar M. Algubili & Aseel M. Aljeboree (2016): Synthesis, characterization, and photocatalytic activity of sonochemical/hydration–dehydration prepared ZnO rod-like architecture nano/microstructures assisted by a biotemplate, Environmental Technology, DOI: 10.1080/09593330.2016.1246615

To link to this article: http://dx.doi.org/10.1080/09593330.2016.1246615

Published online: 25 Nov 2016.

ENVIRONMENTAL TECHNOLOGY, 2016
http://dx.doi.org/10.1080/09593330.2016.1246615

Taylor & Francis
Taylor & Francis Group

Synthesis, characterization, and photocatalytic activity of sonochemical/hydration–dehydration prepared ZnO rod-like architecture nano/microstructures assisted by a biotemplate

Ayad F. Alkaim [a,b], Enas M. Alrobayi[c], Abrar M. Algubili[d] and Aseel M. Aljeboree[a]

[a]Department of Chemistry, College of Science for Women, Babylon University, Hilla, Iraq; [b]Institut für Technische Chemie, Leibniz Universität Hannover, Hannover, Germany; [c]Department of Laser Physics, College of Science for Women, Babylon University, Hilla, Iraq; [d]Department of Pharmacy, College of Pharmacy, Kufa University, Najaf, Iraq

ABSTRACT

ZnO nanoparticles of rod-like architecture have excellent potential to be used in wastewater treatment as a photocatalyst. They were synthesized by utilizing sonochemical/hydration-dehydration techniques using glutamine as a biotemplate. The effects of calcination temperatures, that is, 300°C, 500°C, and 700°C, on the crystallinity, optical properties, and photocatalytic activity of synthesized zinc oxide nanoparticles were investigated. X-ray diffraction (XRD) results indicated that all calcinated samples have a crystalline hexagonal wurtzite structure. Morphology and elemental compositions were investigated using field emission-scanning electron microscopy with energy-dispersive X-ray spectroscopy. The XRD and Fourier transform infrared (FTIR) spectra revealed that the samples were amorphous at 100°C; however, it changed into a crystalline structure amid the calcination process. Optical properties were determined using a UV-visible reflection spectrophotometer and showed abatement in the band gap with increasing annealing temperature. The progress of the photocatalytic degradation was monitored by a UV-visible spectrophotometer, while the mineralization ability was estimated by total organic carbon tests of ZnO-calcinated samples. The effect of various operational parameters the photocatalytic efficiency and rate of dye degradation was studied. High photocatalytic degradation of maxilon blue dye (GRL) was found at pH 6.3.

ARTICLE HISTORY
Received 21 June 2016
Accepted 4 October 2016

KEYWORDS
Hierarchical ZnO; nanoparticles; maxilon blue dye; photocatalytic; mineralization

1. Introduction

Wastewaters from the textile, paper, and some different industries contain lingering colors, which are generally nonbiodegradable [1]. As a result of their complex molecular structures, poor biodegradability, and high solubility, it is very hard to remove dyes from aqueous solutions. Consequently, the primary source of aquatic environmental pollution, considerable a color wastewater represents in ecology systems. There are different processes that are applied for the treatment of dye waste effluents (physical or chemical) such as adsorption processes [2,3]. However, the pollutants cannot be converted directly into harmless substances in the wastewater by the adsorption process, because these dye effluents are stable to light and oxidizing agents [4]. Thus, the expulsion of these poisonous contaminants from wastewater has attracted immense interest, and many endeavors have been coordinated toward the improvement of productive and financially savvy treatment strategies [5].

In the last few decades, advanced oxidation processes have been successfully used for the degradation and mineralization of harmful pollutants [6,7]. Photocatalysis, a protuberant off-shoot of advanced oxidation processes, has emerged as one of the most efficient methods for the complete mineralization of toxic organic pollutants [8,9]. The use of low-cost resources such as semiconductor materials, water, and light photons for the generation of reactive oxygen species (ROS) further authenticates its efficacy and economic viability [10]. To date, photocatalytic nanomaterials, including metal oxides, have been used for the photocatalytic degradation of contaminants [11–15]. However, most reported photocatalysts have some disadvantages, which make them unsuitable for any practical applications in wastewater, due to their high cost, low photocatalytic efficiency, and difficulty to be recycled.

CONTACT Ayad F. Alkaim alkaimayad@gmail.com; ayad_alkaim@yahoo.com; alkaim@iftc.uni-hannover.de Institut für Technische Chemie, Leibniz Universität Hannover, Callinstrasse 3, D-30167 Hannover, Germany

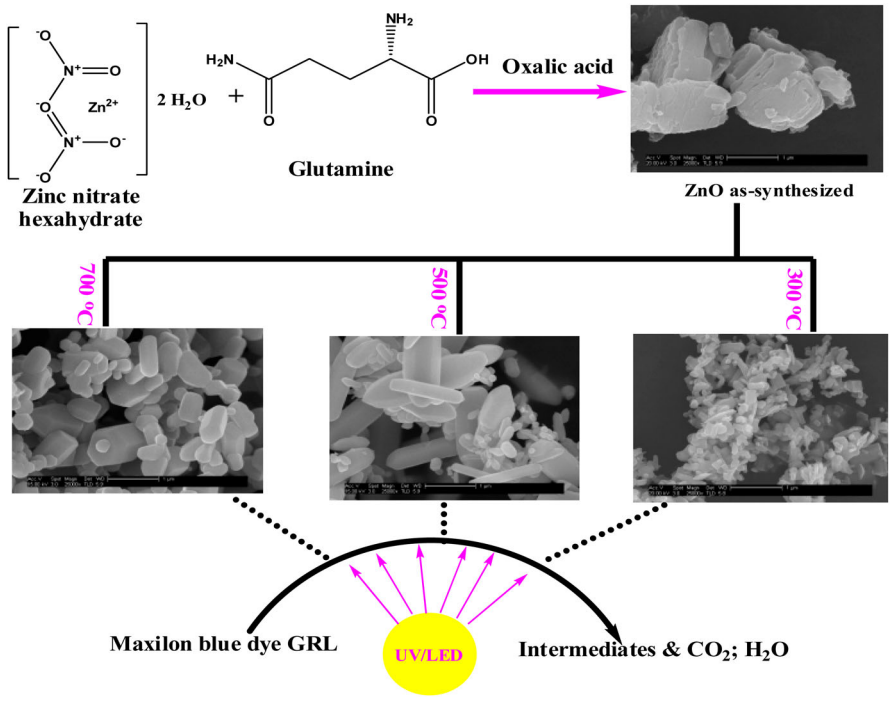

Scheme 1. Schematic representation of the research work.

Comparatively, TiO_2 and ZnO nanomaterials show the most promising applications in the environmental treatment field due to their low cost, high photocatalytic efficiency, and environmental sustainability [16–19].

In comparison with TiO_2, ZnO shows two important advantages: less charge recombination and higher light absorption below 400 nm [20]. Due to its high photocatalytic activity, ZnO is also one of the most extensively used photocatalysts, and is used in both acidic and basic media [21,22]. Some organic template additives were found to enhance the properties of ZnO [23]. This is mostly because of their impact by enhancing the physical, chemical, optical, and electrical properties. A portion of the broadly utilized organic templates are polyalkene glycol, triethyl amine, egg white, and ethylene glycol [24,25].

However, there are very few reports on the utilization of biotemplates for the synthesis of ZnO nanostructures [26]. Here, we endeavor to find a more easy method for the synthesis, characterization, and determination of the photocatalytic efficiency of ZnO nanopowder obtained by using glutamine as a friendly and nontoxic biotemplate, and water as a green solvent-assisted sonochemical/hydration–dehydration process. To the best of our knowledge, the use of glutamine as a biotemplate for the synthesis of ZnO has not been reported. In this paper, we developed a new and simple synthesis with high photocatalytic properties via sonochemical/hydration–dehydration assisted by a biotemplate-free aqueous solution method. We also demonstrate the effects of different annealing temperatures of the prepared ZnO nanoparticles on their morphology, structural characteristics, and photocatalytic activity.

The photocatalytic efficiency of the synthesized ZnO was evaluated by photocatalytic removal/mineralization of aqueous maxilon blue dye. A schematic representation of the research work is presented in Scheme 1.

2. Experimental details

2.1. Chemical synthesis of ZnO nanorods

ZnO nanoparticles are usually synthesized by the sonochemical/hydration–dehydration method using $Zn(NO_3)_2{\cdot}6H_2O$, $H_2C_2O_4$, and glutamine (purchased from Sigma-Aldrich Company). All chemicals were used in the synthesis process without any further purification.

An appropriate amount of zinc nitrate $Zn(NO_3)_2{\cdot}6H_2O$ (2 mol was first dissolved in 100 mL of deionized water; the solution was rapidly stirred using a magnetic stirrer,), 5.0 g of $H_2C_2O_4{\cdot}5H_2O$, and 4.0 g of glutamine were separately dissolved in 50 mL deionized water. Zinc nitrate and oxalic acid components were mixed in a reaction container using an ultrasonic bath with at a frequency of 37 kHz for 60 min (ultrasonic irradiation was accomplished with an Elmasonic P ultrasonic cleaning unit (bath ultrasonic) at a frequency of 37 kHz and 100% output power). Glutamine solution was added dropwise to this mixed solution with continuous ultrasonic effect. Immediately, the suspension containing the precursor of ZnO turned milky white, which indicated

the formation of ZnO nanoparticles. This was followed by a simple evaporation and drying (hydration/dehydration method) process modified from previous procedures in the literature [27]. The suspension containing ZnO nanoparticles was heated to 70°C for 10 h until complete evaporation of water; ZnO nanoparticles were repeatedly washed several times with ethanol and deionized water to remove ionic impurities and filtered. Thereafter, the precipitate was collected by decantation and dried at 100°C overnight. The ZnO nanoparticles were then annealed in an electric furnace at 300°C, 500°C, or 700°C for 2 h under an air atmosphere and cooled to room temperature naturally. The resulting samples were labeled as ZnO-G300, ZnO-G500, and ZnO-G700.

2.2. Analytical instruments

ZnO nanoparticles ZnO-G300, ZnO-G500, and ZnO-G700 were characterized by using different characterization techniques. Powder-X-ray diffraction (XRD) patterns of the ZnO photocatalysts were recorded by a Bruker AXS D4 Endeavor diffractometer using a reflection geometry with fixed divergence slits and Cu-Kα radiation (λ = 0.15418 nm). To determine the particle size and element type, field emission-scanning electron microscope (FE-SEM) images and corresponding energy-dispersive (EDX) spectroscopy were taken with an FE-SEM (JEOL JSM-6700F, Japan). Transmission versus cm^{-1} was studied by FTIR Model M 2000 Midac, U.S.A. Ultraviolet diffuse reflectance measurement was carried out to measure the band-gap energy, which was recorded with a UV–vis spectrophotometer (Varian Cary 100) equipped with a Labsphere integrating sphere diffuse reflectance accessory.

2.3. Photocatalytic degradation

The synthetic wastewater containing maxilon blue dye (GRL) using a test of photocatalytic activity for prepared ZnO nanorods under the illumination of UVA light. LED UV (A) 365 nm/Thorlab, U.S.A., using as a light source of photocatalytic degradation. The incident photon flux measured by UVA radiometer, Dr Honle/Germany, was switched on after three minutes. The molecular structure of GRL is shown in Figure 1. All the experiments were carried out at 25 ± 3°C. The pH of dye solutions was adjusted by adding 0.1 M HNO_3 or NaOH using IQ scientific experiment pH meter. The solution was continuously stirred for 30 min in a dark environment to reach the adsorption/desorption equilibrium of GRL dye over the surface of ZnO nanorods. At varied time intervals, 3 mL of the dispersion was extracted from the sample and centrifuged at 3500 rpm for 10 min.

The change in concentration of the centrifuged dye solutions was evaluated by measuring the relative intensity of UV–visible absorbance at 605 nm using a UV 1650 spectrometer (Shimadzu, Japan). The removal rate of photodegradable dye was calculated as C_t/C_0, where C_0 is the initial concentration and C_t is the concentration of centrifuged GRL dye solution (mg/L).

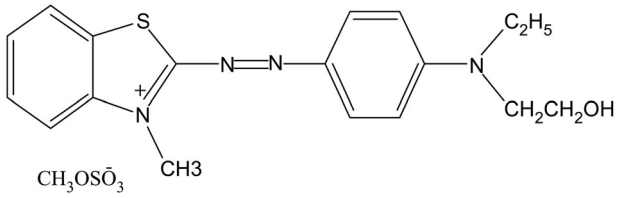

Figure 1. Molecular structure of maxilon blue dye GRL.

Unless otherwise specified, all the experiments were done at natural pH of GRL (6.3). The effect of various operational parameters such as calcination temperature (300°C, 500°C, and 700°C), amount of catalyst (0.25–5.00 g/L), concentration of dye (10–200 mg L^{-1}) and pH (3–10) of dye solution on the photocatalytic efficiency and rate of dye degradation was studied. Moreover, the effect of electron scavengers on photocatalytic degradation was also investigated, and high photocatalytic degradation of maxilon blue dye GRL was found at pH 6.3.

3. Results and discussion

3.1. Characterizations of synthesized ZnO nanorods

XRD was used to investigate the phase and purity of the as-synthesized ZnO and aid by three types of calcination temperatures. Figure 2(a) shows the XRD patterns of the as-synthesized ZnO; the amorphous character has been

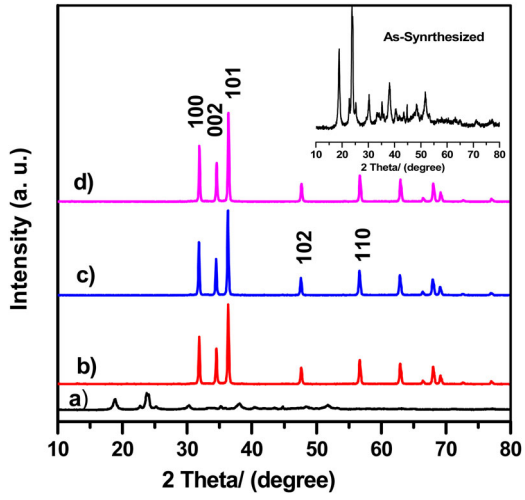

Figure 2. The XRD diffractogram of zinc oxide nanoparticles at different annealing temperatures (a) as-synthesized, (b) ZnO-G300, (c) ZnO-G500, and (d) ZnO-G700.

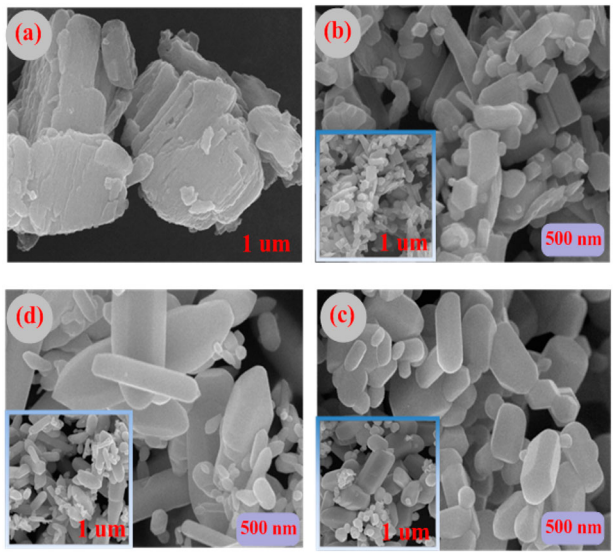

Figure 3. FE-SEM images of ZnO nanorods (a) as-synthesized, (b) ZnO-G300, (c) ZnO-G500, and (d) ZnO-G700.

indicated to have resulted from the organic glutamine and oxalic acid residues. Less intense peaks were found at the 2θ values from 20° to 40°, which attributed to the presence of a minor crystalline phase of Zn-glutamine organo–inorganic complexes [26]. After calcinations, the characteristic peaks (Figure 2(b–d)) can be matched to the hexagonal structure of wurtzite ZnO detected according to the standardized JCPDS card (no. 36–1451) [28,29]. All calculations of crystal size depend on the peak (101) plane. The (101) plane had high purity and strongest line for all studied samples within annealing temperatures. The highest stronger diffraction peaks of ZnO-G500 has been investigated, indicating that the shape of ZnO nanoparticles well crystallized with the annealing temperature [29,30].

The morphology of ZnO samples was observed by using FE-SEM. As shown in Figure 3, ZnO-G300 exhibits as 'chemical sedimentary rocks' due to the agglomeration of nanoparticles (Figure 3(a)), whereas the FE-SEM in Figure 3(b) and in the inset of Figure 3(b) indicate that ZnO-G300 has a shape of nanorods with some irregular composed. Figure 3(c,d) and the inset of Figure 3(c, d) show a clearer morphology of ZnO nanorods (ZnO-G500 and ZnO-G700), respectively; this is attributed to that the annealing temperature which plays an important role in determining the structure and morphology of ZnO; the same behavior has been found in previous published works [30–32].

The elemental analysis of the synthesized ZnO samples were confirmed by EDX, which shows the presence of atomic percentages of oxygen and zinc as illustrated in Table 1, with higher concentration of Zn, which is attributed to high oxygen vacancies [33].

Table 1. EDX analysis results of ZnO nanorods at different annealing temperatures.

	ZG3		ZG5		ZG7	
Element	Weight %	Atomic %	Weight %	Atomic %	Weight %	Atomic %
O	19.66	48.77	18.46	45.75	16.3	40.4
Zn	80.34	51.22	81.54	54.24	83.7	59.56
Total	100	100	100	100	100	100

To complement XRD, FTIR spectra were performed of ZnO as-synthesized and annealing samples, and the results are shown in Figure 4. It is clear from the results that the absorption peak between 2344 and 2352 cm^{-1} indicates the existence of CO_2 molecules in air [34]. Since the measurement was carried out at room temperature under air atmosphere, the absorption of H_2O from moisture content and CO_2 from the atmosphere is unavoidable. The broad absorption peaks at ~3480 and ~1607 cm^{-1} can be assigned to the presence of hydroxyl groups in the absorbed water (Figure 4(a)); these peaks disappear with increasing annealed temperatures (Figure 4(b–d)) due to the removal of absorbed water [35,36]. The well-resolved intense and broad transmission band below ~520 cm^{-1} was attributed to the stretching vibration of zinc–oxygen bond [37,38].

The optical properties of ZnO samples were examined at room temperature by using UV–Vis diffuse reflectance spectra, shown in Figure 5. It can be clearly evidence that all samples show an absorption strong edges around 370–380 nm, which can be caused by the intrinsic band-gap absorption of ZnO, revealing to the electron transitions from the valence band to the conduction band (CB) ($O_2p \rightarrow Zn_3d$) [39,40].

Optical band-gap energies were determined using the Kubelka–Munk function by extrapolation of the linear part

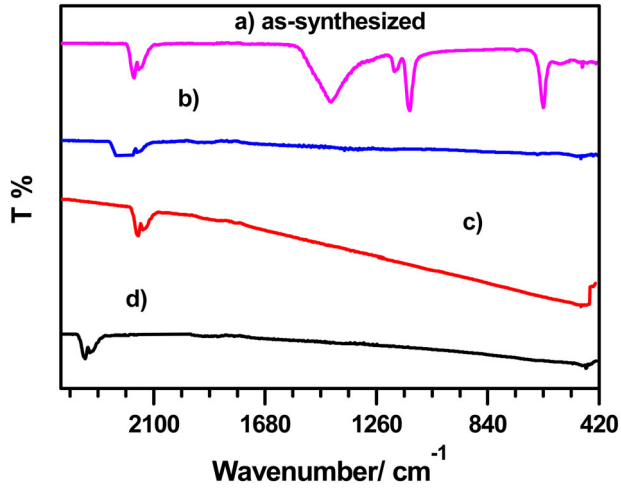

Figure 4. FTIR spectra of ZnO nanorods (a) as-synthesized, (b) ZnO-G300, (c) ZnO-G500, and (d) ZnO-G700.

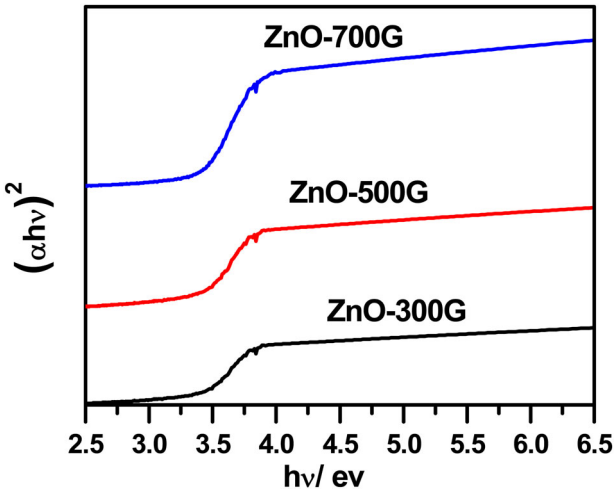

Figure. 5. UV–visible absorption spectrum of ZnO nanoparticles.

of the plot between the $(F(R)E^{1/2})$ versus the energy of the absorbed light (hv) [41]. The obtained Eg values are 3.23, 3.22, and 3.20 eV as the temperature increased from 300°C to 700°C, respectively. Compared to the reported values of band-gap energy of bulk ZnO (Eg = 3.37 eV) [42], the optical absorption edge slightly shifted toward red wavelength, which may be induced by more defects appearing at higher annealing temperatures [43].

3.2. Effect of different parameters on photocatalytic activity

3.2.1. Calcination temperature

Calcination temperature has a prominent effect on the efficiency of the prepared photocatalysts; therefore, the influence of the calcination temperature on the photocatalytic activity of irradiated maxilon blue dye GRL by UVA light was examined. The ZnO nanoparticles were subjected to various calcination temperatures ranging from 300°C to 700°C.

It is clear from the results shown in Figure 6(a,b) that the photocatalytic activity of the prepared samples increased with an increase in the calcination temperature from 300°C to 500°C. At 500°C, the photocatalytic efficiency reached the maximum, which is attributed to the change in size and particle morphology of the ZnO surface [33], or might be due to the enhancement of the crystallization, which is beneficial because it reduces the recombination of photo-generated electrons

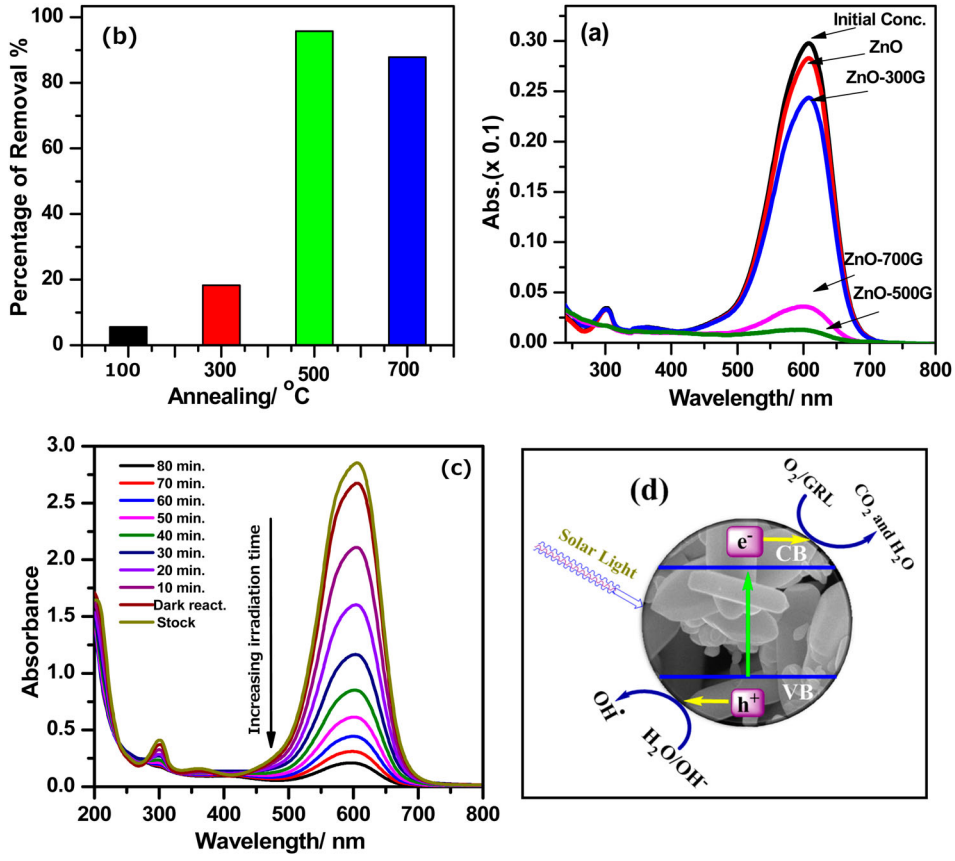

Figure 6. (a) UV–visible absorbance spectra, (b) percentage of photodegradation removal (%) of decomposed GRL dye solution at different annealing temperatures of synthesized ZnO under UVA, (c) UV–visible absorbance spectra with respect to time intervals, and (d) a schematic illustration of GRL dye photodegradation by ZnO annealing at 500°C (ZnO-G500).

and holes [44]. In addition, with further increase in the calcination temperature from 500°C to 700°C, the photocatalytic activity decreases. The time-dependent electronic absorption spectrum of maxilon blue dye GRL during photoirradiation in the presence of ZnO-G500 is presented in Figure 6(c); the absorption intensity decreases with an increase in the irradiation time. Besides, no new bands were detected in the UV–vis region due to the photodegradation process. Furthermore, Figure 6(d) exhibits the suggested mechanism under UVA irradiation for the degradation of GRL in the presence of ZnO-G500 as a photocatalyst; for the desired reaction, the energy required to promote an electron (ē) from the valance band (VB) to the CB of ZnO-G500 upon light illumination is equal to or higher than the band-gap energy. The created photo-excited ē at the CB of ZnO-G500 produces radicals such as superoxide anion O_2^-due to the interaction with surface oxygen. At the VB side, active oxygenated species such as OH radicals are produced by the reaction of either H_2O or ^-OH species with h^+ forms on the ZnO surface; these steps lead to the photocatalytic degradation and mineralization of the organic pollutant [45].

The mineralization of the maxilon blue dye GRL by using different samples of ZnO photocatalysts was checked with a total organic carbon (TOC) analyzer, and the results are depicted in Figure 7. The results showed that TOC was removed with difficulty after 180 min of irradiation; in this time the GRL dye completely degraded, while only 18.03%, 29.19%, 48.54%, and 41.34% TOC for ZnO (as synthesized), ZnO-G300, ZnO-G500, and ZnO-G700, respectively, indicating some of the intermediate un-degradable organic species, remained in the solution [46].

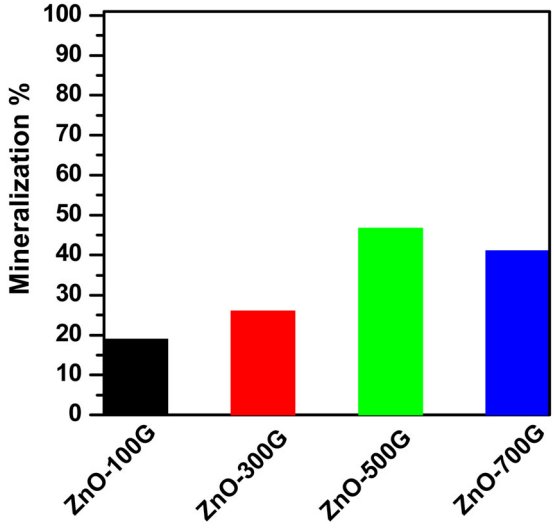

Figure 7. Effect of annealing temperature on photocatalytic mineralization of GRL dye catalyzed by ZnO: catalyst amount 1.5 g L^{-1}; pH of solution 6.3; GRL dye concentration (100 mg L^{-1}); and irradiation time (degradation = 180 min).

3.2.2. Radical scavenger

During the photocatalytic degradation of maxilon blue GRL, both the photo-generated holes and electrons can produce ROS. Therefore, to further understand the role of the ROS ($OH^\bullet$, $O_2^{\bullet -}$ or h^+) involved and to check their impact on the photocatalytic degradation of GRL dye under UVA light, hole scavengers and radical scavengers were added to the reaction of the photocatalytic degradation process. The reaction mechanism of maxilon blue dye photocatalytic degradation through the generation of ROS can be described in thefollowing equations:

$$ZnO + GRL \xrightarrow{Adsorption} GRL/ZnO, \quad (1)$$

$$GRL/ZnO + hv \rightarrow GRL/ZnO(e_{CB}^- + h_{VB}^+), \quad (2)$$

$$ZnO(h_{VB}^+) + H_2O \rightarrow OH^\bullet + H^+, \quad (3)$$

$$ZnO(h_{VB}^+) + OH^- \rightarrow OH^\bullet, \quad (4)$$

$$ZnO(e_{CB}^-) + O_2 \rightarrow O_2^{\bullet -}, \quad (5)$$

$$OH^\bullet + GRL \rightarrow Intermediate\ \ Product \rightarrow Degradation, \quad (6)$$

$$O_2^{\bullet -} + GRL \rightarrow Intermediate\ \ Product \rightarrow Degradation. \quad (7)$$

Initially, GRL molecules are adsorbed onto the ZnO surface, after that the suspension of GRL/ZnO is irradiated by a chosen wavelength, generating CB electron (e^-) and valence band holes (h^+) [47]. To further understand the photocatalytic degradation mechanism, several scavengers were used; as the $OH^\bullet$ radical scavenger isopropanol (IPA) was added [48], *n*-phenyl aniline (DPA) was introduced as the scavenger of $O_2^{\bullet -}$ [49] and potassium iodide (KI) was added as a scavenger of both h^+ and $OH^\cdot$ [50].

The results are shown in Figure 8. Shows the radical species plays a major role in the photocatalytic degradation of GRL, the degradation efficiency is expected to decrease greatly. The poorest results were observed with in the presence of KI, which could capture the reactive species (e.g. both h+ and $OH^\bullet$, more as hydroperoxylHOO$^\cdot$ radicals) to inhibit the photocatalytic activity. Moreover, the lowest GRL dye photocatalytic degradation efficiency suggested indirectly that both h^+ and $OH^\cdot$ are considered as a very important reactive species in the photocatalytic process. On the other hand, compared with KI, photocatalytic degradation in the presence of DPA or IPA still played a vital function, but was less effective than $OH^\cdot$ [51,52].

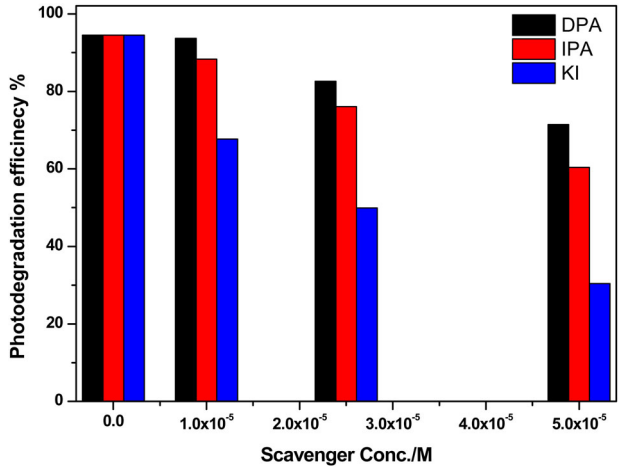

Figure 8. Effect of scavenger concentration on photocatalytic degradation GRL dye catalyzed by ZnO-G500: catalyst amount 1.5 g L^{-1}; pH of solution 6.3; GRL dye concentration (100 mg L^{-1}); and irradiation time (degradation = 60 min).

3.2.3. Catalyst loading

The effect of photocatalyst loading on GRL removal using ZnO-G500 photocatalyst was investigated by varying the amount of photocatalyst. It was observed initially that the photodegradation efficiency increased with an increase in the amount of the photocatalyst until a certain limit up to 1.5 g L^{-1}, after that it slightly decreased (Figure 9).

This phenomenon could be attributed to the increase in active sites with the increase in ZnO-G500, which is responsible for the enhanced photocatalytic activity [53].

Indeed, improvement in the removal efficiency is not obvious with further increase in the ZnO dosage.

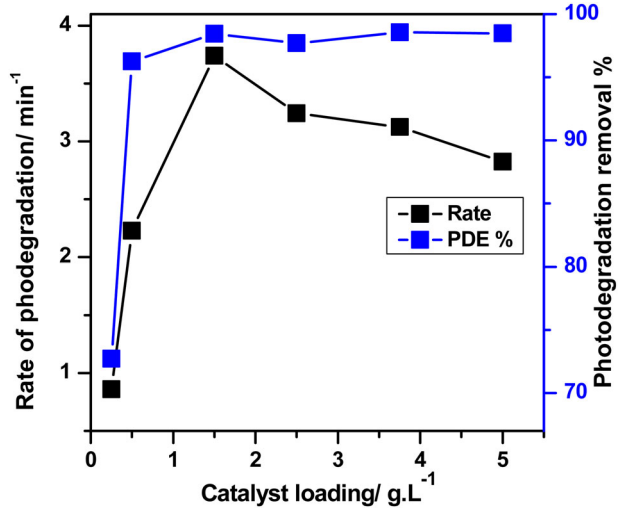

Figure 9. Effect of catalyst dosage on the photocatalytic degradation of GRL dye catalyzed by ZnO-G500: pH of solution 6.3; GRL dye concentration (100 mg L^{-1}); and irradiation time (degradation = 60 min).

However, high amount of ZnO nanoparticles became much easier to aggregate and reduced the light transmission [54,55]. Furthermore, activated ZnO may be deactivated through collision with ground-state catalysts as follows:

$$ZnO^{*} + ZnO \xrightarrow{\text{collision}} ZnO^{\#}; + ZnO, \quad (8)$$

where ZnO^{*} and $ZnO^{\#}$; are the activated and deactivated forms of ZnO, respectively.

3.2.4. pH of solution

The pH of the solution is an important parameter in photocatalytic degradation reactions, because the generation of hydroxyl radicals is considered as a function of pH. Therefore, the degradation of dye was studied at different pHs of the solution in acid, neutral, and alkaline media, which is shown in Figure 10, and indicated that the degradation rate and the photocatalytic removal efficiency of GRL in a neutral medium are higher than that in an acid or alkaline medium.

The observed trends from Figure 10 are clearly related to the electrostatic interactions which can be changed depending on the chemical nature between the substrate GRL and the photocatalyst ZnO nanoparticle surface, which depends on the pH point of zero charge (pHpzc) and the pH of substrate. Comparing the rate of photocatalytic degradation and photodegradation efficiency of GRL dye at different pH values, we conclude that the degradation seems to be slow in both acidic and basic media. However, the highest degradation of the GRL dye occurs at pH = 6.5.

Thus, when the pH values are below the pHpzc, the catalyst particles are protonated and become positively charged [56,57]. However, when the pH values are above the pHpzc, the catalyst particles are deprotonated and become negatively charged [58,59]. The pHpzc of ZnO nanoparticles is about 9. Additionally, the GRL dye has a neutral pH. Therefore at acidic pH, both ZnO nanoparticles surface and GRL dye are positively charged and the same polarity of charge results in an electrostatic repulsion between them, which reduces the adsorption on the catalyst surface. At pH between 6.5 and 7.5, the GRL has a neutral charge, whereas the ZnO photocatalyst has a negative charge, favoring the adsorption and it is responsible for the high degradation. At pH > 8.5, both GRL and ZnO are negatively charged, so the repulsive forces between the catalyst and the molecule are developed.

3.2.5. Initial dye concentration

The dependence of photocatalytic degradation efficiency on the initial concentration of maxilon blue dye was investigated; the experiment was repeated at a range of initial dye concentration from 10 to

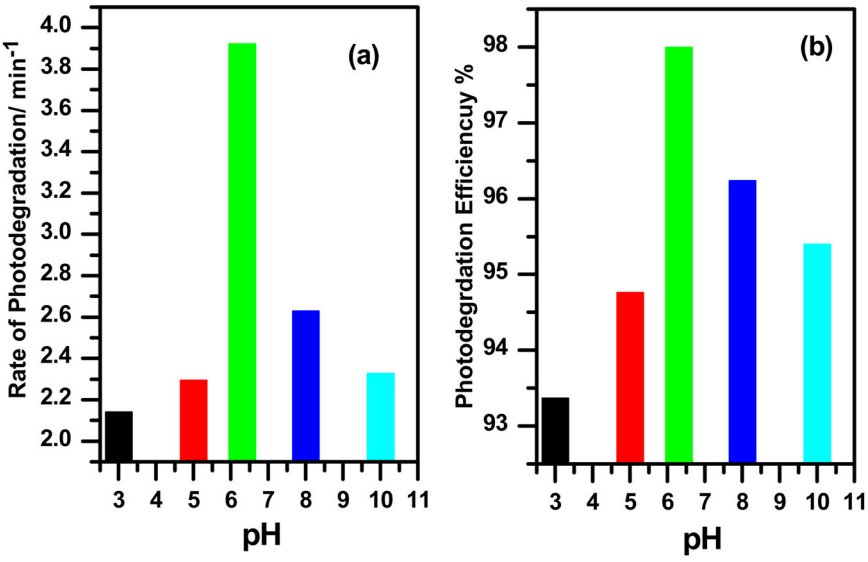

Figure 10. Influence of initial solution pH on the photocatalytic degradation of GRL dye catalyzed by ZnO-G500: catalyst suspended = 1.5 g L^{-1}; GRL dye concentration (100 mg L^{-1}); and irradiation time (60 min).

200 mg L^{-1} (Figure 11(a)). High values of (R^2) were obtained from the nonlinear line relationship of C_t/C_0 versus irradiation time *t*. This behavior of photocatalytic degradation indicates a first-order expression up to an initial concentration of GRL dye.

Data on the rate constant obtained from Figure 11(a) were then fitted to the Langmuir–Hinshelwood (L–H) kinetics rate model, which has been applied to analyze the concentration of pollutants as a function of the initial rates of photocatalytic degradation [57,60,61]. The rate law is shown in the following equation:

$$r = \frac{dC}{dt} = \frac{k_L K_{ads} C_0}{1 + K_{ads} C_0} \quad . \tag{9}$$

The applicability of the L–H equation for degradation has been confirmed by the nonlinear plot model (R^2 of 0.9359), obtained for rate of photocatalytic degradation versus initial concentration (Figure 11(b)). This indicates that the degradation of GRL occurred mainly on the surface of ZnO and fitted well to the L–H model. The values of *k* and *K*, determined from the nonlinear expression of the plot, are 4.194×10^3 g L^{-1} min^{-1} and 8.93×10^{-5} L g^{-1}, respectively.

Based on the results in Figure 11(a), the photocatalytic degradation efficiency is very high at low concentrations of the maxilon blue dye, and then, as the dye concentration increases, it gradually decreases. This might be attributed to a competition of adsorption between dye molecules (e.g. GRL) and dissolved O_2 into the catalyst surface (e.g. ZnO). As O_2 molecules are the electron acceptors in the photocatalytic reaction, therefore, lesser the O_2 adsorbed than the dye on the catalyst surface, lesser is the degradation efficiency as well as the rate constant [11]. Another possible cause for such results is the effect of UV-screening of the dye itself, because a very low amount of UV may be absorbed by the ZnO nanoparticles

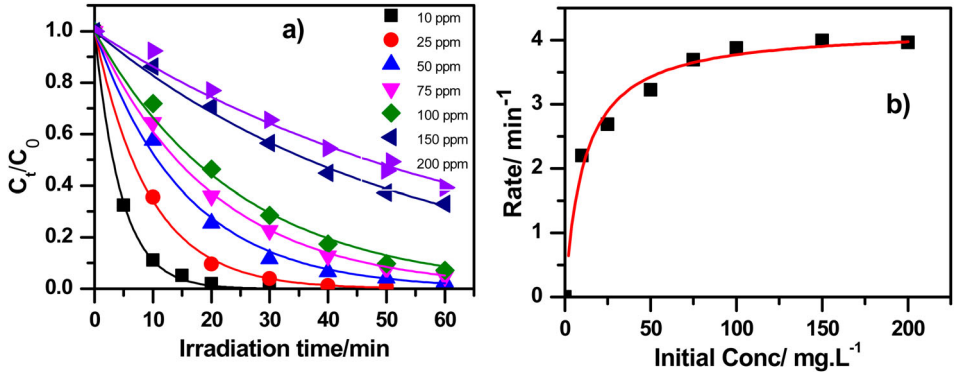

Figure 11. (a) Kinetics of nonlinear fit, and (b) L–H model of photocatalytic degradation of GRL dye catalyzed by ZnO-G500: catalyst suspended = 1.5 g L^{-1}; pH 6.3; irradiation time (60 min); and L.I. 2 mW cm^{-2}.

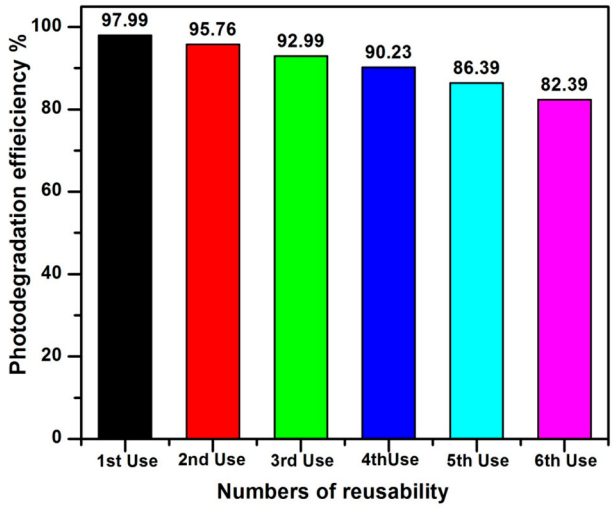

Figure 12. The reusability of ZnO-G500 photocatalyst: catalyst suspended = 1.5 g L^{-1}, GRL dye concentration (100 mg L^{-1}), pH of solution 6.5, and irradiation time (60 min).

at a high dye concentration, which reduces the photocatalytic efficiency of the surface reaction [52].

3.2.6 Reusability of catalyst

To study the stability of ZnO-G500 photocatalyst, ZnO nanoparticles were recovered from the reaction mixture by filtration and reused six times under similar reaction conditions: the usage of ZnO-G500 (1.5 g L^{-1}), GRL dye concentration (100 mg L^{-1}), pH of the solution (6.5), and irradiation time (60 min). After the completion of the first run of the photocatalytic degradation experiment, ZnO-G500 was collected through filtration, washed several times using deionized water, then dried for 4 h at 100°C, and the product was used in the next photocatalytic degradation experiment. The results of the first experiment and five repeated experiments are shown in Figure 12. It was observed that after reuse, ZnO-G500 nanoparticles showed lower photocatalytic activity: the photodegradation efficiency dropped from 97.99% of the 1st use to 82.39% of the 6th repeated use. This result illustrates that the surface of ZnO-G500 nanoparticles showed very good stability.

4. Conclusion

In this work, a green precursor-based economical and convenient method for preparing ZnO nanorods by sonochemical/hydration–dehydration method using glutamine as a biotemplate was investigated. The effects of annealing temperature on ZnO nanoparticles with respect to the morphological characteristics were investigated. XRD results confirmed that the ZnO nanoparticles have pure hexagonal wurtzite structure. FE-SEM micrographs show that the particle size was temperature dependent; therefore, the average crystallite size increased with increasing calcination temperature for the ZnO samples. The best photocatalytic performance in the degradation of GRL was found to be ZnO-G500 > ZnO-G700 > ZnO-G300 > ZnO as-synthesized, respectively. Photodegradation of GRL dye by ZnO nanoparticles was studied thoroughly and the effect of various parameters such as effect of solution pH, catalyst loading, and initial dye concentration was also investigated. The applicability of the L–H kinetic model reveals that the degradation of maxilon blue dye occurs mainly on the surface of the photocatalyst.

Acknowledgements

The authors would like to thank University of Northampton, UK, for the material characterizations.

Disclosure statement

No potential conflict of interest was reported by the authors.

ORCID

Ayad F. Alkaim http://orcid.org/0000-0003-3459-4583

References

[1] Chakrabarti S, Dutta BK. Photocatalytic degradation of model textile dyes in wastewater using ZnO as semiconductor catalyst. J Hazard Mater. 2004;112:269–278.
[2] Alkaim AF, Sadik Z, Mahdi DK, et al. Preparation, structure and adsorption properties of synthesized multiwall carbon nanotubes for highly effective removal of maxilon blue dye. Kor J Chem Eng. 2015;32:2456–2462.
[3] Aljeboree AM, Alkaim AF, Al-Dujaili AH. Adsorption isotherm, kinetic modeling and thermodynamics of crystal violet dye on coconut husk-based activated carbon. Desalin Water Treat. 2015;53:3656–3667.
[4] Galindo C, Jacques P, Kalt A. Photooxidation of the phenylazonaphthol AO20 on TIO_2: kinetic and mechanistic investigations. Chemosphere. 2001;45:997–1005.
[5] Wang H-J, Sun Y-Y, Cao Y, et al. Porous zinc oxide films: controlled synthesis, cytotoxicity and photocatalytic activity. Chem Eng J. 2011;178:8–14.
[6] Hoffmann MR, Martin ST, Choi W, et al. Environmental applications of semiconductor photocatalysis. Chem Rev. 1995;95:69–96.
[7] Gaya UI, Abdullah AH. Heterogeneous photocatalytic degradation of organic contaminants over titanium dioxide: a review of fundamentals, progress and problems. J Photochem Photobiol C. 2008;9:1–12.
[8] Alkaim AF, Kandiel TA, Hussein FH, et al. Enhancing the photocatalytic activity of TiO_2 by pH control: a case study for the degradation of EDTA. Catal Sci Technol. 2013;3:3216–3222.

[9] Park J-Y, Hwang K-J, Lee J-W, et al. Fabrication and characterization of electrospun Ag doped TiO_2 nanofibers for photocatalytic reaction. J Mater Sci. 2011;46:7240–7246.
[10] Kumar SG, Rao KK. Zinc oxide based photocatalysis: tailoring surface-bulk structure and related interfacial charge carrier dynamics for better environmental applications. RSC Adv. 2015;5:3306–3351.
[11] Saikia L, Bhuyan D, Saikia M, et al. Photocatalytic performance of ZnO nanomaterials for self sensitized degradation of malachite green dye under solar light. Appl Catal A-Gen. 2015;490:42–49.
[12] Lee KM, Abdul Hamid SB, Lai CW. Multivariate analysis of photocatalytic-mineralization of eriochrome black T dye using ZnO catalyst and UV irradiation. Mater Sci Semicond Process.2015;39:40–48.
[13] Hemalatha K, Ette PM, Madras G, et al. Visible light assisted photocatalytic degradation of organic dyes on TiO_2–CNT nanocomposites. J Sol-Gel Sci Technol. 2015;73:72–82.
[14] Gnanaprakasam A, Sivakumar VM, Sivayogavalli PL, et al. Characterization of TiO_2 and ZnO nanoparticles and their applications in photocatalytic degradation of azodyes. Ecotox Environ Safe. 2015;121:121–125.
[15] Shie J, Lee C, Chiou C, et al. Photocatalytic characteristic and photodegradation kinetics of toluene using N-doped TiO_2 modified by radio frequency plasma. Environ Technol. 2014;35:653–660.
[16] Li Y, Xie W, Hu X, et al. Comparison of dye photodegradation and its coupling with light-to-electricity conversion over TiO_2 and ZnO. Langmuir. 2010;26:591–597.
[17] Akhmal Saadon S, Sathishkumar P, Mohd Yusoff AR, et al. Photocatalytic activity and reusability of ZnO layer synthesised by electrolysis, hydrogen peroxide and heat treatment. Environ Technol. 2016;37:1875–1882.
[18] Alkaim AF, Dillert R, Bahnemann DW. Effect of polar and movable (OH or NH_2 groups) on the photocatalytic H_2 production of alkyl-alkanolamine: a comparative study. Environ Technol. 2015;36:2190–2197.
[19] Alkaim AF, Kandiel TA, Dillert R, et al. Photocatalytic hydrogen production from biomass-derived compounds: a case study of citric acid. Environ Technol. 2016;37:2687–2693.
[20] Ling T, Song J-G, Chen X-Y, et al. Comparison of ZnO and TiO_2 nanowires for photoanode of dye-sensitized solar cells. J Alloys Compd. 2013;546:307–313.
[21] Zhong Jb, Xu B, Feng FM, et al. Fabrication and photocatalytic activity of ZnO prepared by different precipitants using paralled flaw precipitation method. Mater Lett. 2011;65:1995–1997.
[22] Saffar-Teluri A, Bolouk S, Amini M. Synthesis of ZnO microcrystals and their photocatalytic ability in the degradation of textile azo dyes. Res Chem Intermed. 2013;39:3345–3353.
[23] Mohajerani MS, Mazloumi M, Lak A, et al. Self-assembled zinc oxide nanostructures via a rapid microwave-assisted route. J Cryst Growth. 2008;310:3621–3625.
[24] Liu Z, Jin Z, Li W, et al. Preparation of ZnO porous thin films by sol-gel method using PEG template. Mater Lett. 2005;59:3620–3625.
[25] Chen D, Jiao X, Cheng G. Hydrothermal synthesis of zinc oxide powders with different morphologies. Solid State Commun.1999;113:363–366.
[26] Nouroozi F, Farzaneh F. Synthesis and characterization of brush-like ZnOnanorods using albumen as biotemplate. J Braz Chem Soc. 2011;22:484–488.
[27] Miranda SM, Romanos GE, Likodimos V, et al. Pore structure, interface properties and photocatalytic efficiency of hydration/dehydration derived TiO_2/CNT composites. Appl Catal B: Environ. 2014;147:65–81.
[28] Zhou M, Lv W, Liu C, et al. Flower-like and hollow sphere-like ZnO assisted by microorganisms and their UV absorption and photo catalytic performance. J Mater Sci: Mater Electron. 2013;24:36–43.
[29] Wang X, Zhang Y, Hao C, et al. Solid-phase synthesis of mesoporous ZnO using lignin-amine template and its photocatalytic properties. Ind Eng Chem Res. 2014;53:6585–6592.
[30] Raoufi D. Synthesis and photoluminescence characterization of ZnO nanoparticles. J Lumin. 2013;134:213–219.
[31] Naji Aljawfi R, Rahman F, Shukla DK. Effect of the annealing temperature on the structural and magnetic properties of ZnO nanoparticles. Mater Lett. 2013;99:18–20.
[32] Yuan Y, Huang G-F, Hu W-Y, et al. Tunable synthesis of various ZnO architectural structures with enhanced photocatalytic activities. Mater Lett. 2016;175:68–71.
[33] Ashar A, Iqbal M, Bhatti IA, et al. Synthesis, characterization and photocatalytic activity of ZnO flower and pseudo-sphere: nonylphenolethoxylate degradation under UV and solar irradiation. J Alloys Compd. 2016;678:126–136.
[34] Arshad M, Azam A, Ahmed AS, et al. Effect of co substitution on the structural and optical properties of ZnO nanoparticles synthesized by sol-gel route. J Alloys Compd. 2011;509:8378–8381.
[35] Kayani Z, Saleemi F, Batool I. Effect of calcination temperature on the properties of ZnO nanoparticles. Appl Phys A. 2015;119:713–720.
[36] Habibi MH, Mardani M. Effect of annealing temperature on optical properties of binary zinc tin oxide nano-composite prepared by sol-gel route using simple precursors: structural and optical studies by DRS, FT-IR, XRD, FESEM investigations. Spectrochim Acta, Part A. 2015;137:267–270.
[37] Pudukudy M, Yaakob Z. Hydrothermal synthesis of mesostructured ZnO micropyramids with enhanced photocatalytic performance. Superlattice Microst. 2013;63:47–57.
[38] Ashokkumar M, Muthukumaran S. Microstructure, optical and FTIR studies of Ni, Cu co-doped ZnO nanoparticles by co-precipitation method. Opt Mater. 2014;37:671–678.
[39] Saaedi A, Yousefi R, Jamali-Sheini F, et al. Optical and electrical properties of p-type Li-doped ZnO nanowires. Superlattice Microst. 2013;61:91–96.
[40] Part B, Azarang M, Shuhaimi A, et al. Synthesis and characterization of ZnO NPs/reduced graphene oxide nanocomposite prepared in gelatin medium as highly efficient photo-degradation of MB. Ceram Int. 2014;40:10217–10221.
[41] Ismail AA, Bahnemann DW, Bannat I, et al. Gold nanoparticles on mesoporous interparticle networks of titanium dioxide nanocrystals for enhanced photonic efficiencies. J Phys Chem C. 2009;113:7429–7435.

[42] Li D, Hu J, Fan F, et al. Quantum-sized ZnO nanoparticles synthesized in aqueous medium for toxic gases detection. J Alloys Compd. 2012;539:205–209.
[43] Parra MR, Haque FZ. Aqueous chemical route synthesis and the effect of calcination temperature on the structural and optical properties of ZnO nanoparticles. J Mater Res Technol. 2014;3:363–369.
[44] Liu S, Yu J, Jaroniec M. Tunable photocatalytic selectivity of hollow TiO_2 microspheres composed of anatasepolyhedra with exposed {001} facets. J Am Chem Soc. 2010;132:11914–11916.
[45] Lam S-M, Sin J-C, Abdullah AZ, et al. Degradation of wastewaters containing organic dyes photocatalysed by zinc oxide: a review. Desalin Water Treat. 2012;41:131–169.
[46] Zhou K, Hu X-Y, Chen B-Y, et al. Synthesized TiO_2/ZSM-5 composites used for the photocatalytic degradation of azo dye: intermediates, reaction pathway, mechanism and bio-toxicity. J Appl Surf Sci. 2016;383:300–309.
[47] Saien J, Soleymania AR. Degradation and mineralization of direct blue 71 in a circulating upflow reactor by UV/TiO_2 process and employing a new method in kinetic study. J Hazard Mater. 2007;144:506–512.
[48] Martin ST, Lee AT, Hoffmann MR. Chemical mechanism of inorganic oxidants in the TiO_2/UV process: increased rates of degradation of chlorinated hydrocarbons. Environ Sci Technol. 1995;29:2567–2573.
[49] Zhang X, Guo T, Wang X, et al. Facile composition-controlled preparation and photocatalytic application of BiOCl/$Bi_2O_2CO_3$nanosheets. Appl Catal B-Environ. 2014;150–151:486–495.
[50] Zhang X, Sun DD, Li G, et al. Investigation of the roles of active oxygen species in photodegradation of azo dye AO7 in TiO_2 photocatalysis illuminated by microwave electrodeless lamp. J Photochem Photobiol A. 2008;199:311–315.
[51] Ismail L, Rifai A, Ferronato C, et al. Towards a better understanding of the reactive species involved in the photocatalytic degradation of sulfaclozine. Appl Catal B-Environ. 2016;185:88–99.
[52] Song S, Xu L, He Z, et al. Photocatalytic degradation of C.I. Direct Red 23 in aqueous solutions under UV irradiation using $SrTiO_3$/CeO_2 composite as the catalyst. J Hazard Mater. 2008;152:1301–1308.
[53] Behnajady MA, Modirshahla N, Shokri M, et al. The effect of particle size and crystal structure of titanium dioxide nanoparticles on the photocatalytic properties. J Environ Sci Health A. 2008;43:460–467.
[54] Ghule LA, Patil AA, Sapnar KB, et al. Photocatalytic degradation of methyl orange using ZnOnanorods. Toxicol Environ Chem. 2011;93:623–634.
[55] Senthilraja A, Subash B, Dhatshanamurthi P, et al. Photocatalytic detoxification of acid red 18 by modified ZnO catalyst under sunlight irradiation. Spectrochim Acta, Part A. 2015;138:31–37.
[56] Velmurugan R, Swaminathan M. An efficient nanostructured ZnO for dye sensitized degradation of reactive Red 120 dye under solar light. Sol Energy Mater Sol Cells. 2011;95:942–950.
[57] Yanga H, Lia G, Ana T, et al. Photocatalytic degradation kinetics and mechanism of environmental pharmaceuticals in aqueous suspension of TiO_2: a case of sulfa drugs. Catal Today. 2010;153:200–207.
[58] Zhang H, Zhang P, Ji Y, et al. Photocatalytic degradation of four non-steroidal anti-inflammatory drugs in water under visible light by P25-TiO_2/tetraethyl orthosilicate film and determination via ultra performance liquid chromatography electrospray tandem mass spectrometry. Chem Eng J. 2015;262:1108–1115.
[59] Bechambi O, Sayadi S, Najjar W. Photocatalytic degradation of bisphenol A in the presence of C-doped ZnO: effect of operational parameters and photodegradation mechanism. J Ind Eng Chem. 2015;32:201–210.
[60] Zhang X, Wu F, Wu X, et al. Photodegradation of acetaminophen in TiO_2 suspended solution. J Hazard Mater. 2008;157:300–307.
[61] Hamad HA, Sadik WA, Abd El-latif MM, et al. Photocatalytic parameters and kinetic study for degradation of dichlorophenol-indophenol (DCPIP) dye using highly active mesoporous TiO_2 nanoparticles. J Environ Sci. 2016;43:26–39.